

## ABSORPTION OF $p$ MODES BY THIN MAGNETIC FLUX TUBES

REKHA JAIN<sup>1</sup>, BRADLEY W. HINDMAN<sup>2</sup>, DOUG C. BRAUN<sup>3</sup>, AND AARON C. BIRCH<sup>3</sup>

<sup>1</sup> Applied Mathematics Department, University of Sheffield, Sheffield S3 7RH, UK; [R.Jain@sheffield.ac.uk](mailto:R.Jain@sheffield.ac.uk)

<sup>2</sup> JILA and Department of Astrophysical and Planetary Sciences, University of Colorado, Boulder, CO 80309-0440, USA

<sup>3</sup> NWRA CoRA Division, Boulder, CO 80301, USA

Received 2008 September 19; accepted 2009 January 14; published 2009 March 30

### ABSTRACT

We study the interaction between  $p$  modes and the many magnetic fibrils that lace the solar convection zone. In particular, we investigate the resulting absorption of  $p$ -mode energy by the fibril magnetic field. Through mechanical buffeting, the  $p$  modes excite tube waves on the magnetic fibrils—in the form of longitudinal sausage waves and transverse kink waves. The tube waves propagate up and down the magnetic fibrils and out of the  $p$ -mode cavity, thereby removing energy from the incident acoustic waves. We compute the absorption coefficient associated with this damping mechanism and model the absorption that would be observed for magnetic plage. We compare our results to the absorption coefficient that is measured using the local-helioseismic technique of ridge-filtered holography. We find that, depending on the mode order and the photospheric boundary conditions, we can achieve absorption coefficients for simulated plage that exceed 50%. The observed increase of the absorption coefficient as a function of frequency is reproduced for all model parameters.

*Key words:* MHD – Sun: helioseismology – Sun: magnetic fields – Sun: oscillations

*Online-only material:* color figures

### 1. INTRODUCTION

It is now well established that magnetic structures within the solar photosphere are voracious absorbers of acoustic energy. Sunspots can absorb more than 50% of the incoming acoustic wave power and plage regions can absorb up to 20%. Braun et al. (1987, 1988) (see also Braun 1995; Braun & Birch 2008) measured and characterized the absorption for a variety of magnetic structures, including sunspots, plages, and pores. They find that the absorption coefficient is a function of temporal frequency as well as mode order  $n$  and azimuthal order  $m$ . The absorption increases with frequency, saturating at frequencies higher than roughly 4 mHz. Absorption is most efficient for low mode order and low azimuthal order. In addition, significant phase shifts are induced and are strongly dependent on the field distribution of the magnetic structure (i.e., sunspots cause large phase shifts, whereas plage produces negligible shifts).

In the case of sunspots, a variety of mechanisms have been suggested to explain the observed absorption, with mode conversion, resonant absorption, and mode mixing being the leading contenders. Presently, mode conversion is probably the preferred mechanism, but all may play a role. *Mode conversion* is the partial transformation of acoustic energy into slow magnetosonic waves that occurs whenever a sound wave passes through an equipartition layer, a surface in the magnetized atmosphere where the sound speed and Alfvén speed are equal (e.g., Cally & Bogdan 1993; Cally 2000; Crouch & Cally 2003). The slow waves propagate along the field lines removing energy from the acoustic cavity. Therefore, the spawned slow waves damp the incident acoustic wave. Another possibility that has been explored is *resonant absorption* (Hollweg 1988; Lou 1990; Keppens et al. 1994; Rosenthal 1992). Incident acoustic waves can resonantly excite MHD waves in the magnetic structure as long as the magnetic waves have the same wavelength parallel to the magnetic–nonmagnetic interface as the incident wave. Sufficiently high absorption has been difficult to achieve with this mechanism when the atmosphere is stratified because the wave-

lengths are not uniform with height and possess different vertical profiles inside and outside the region of field. *Mode mixing* is the scattering of an incident  $p$  mode of one mode order  $n$  into an outgoing  $p$  mode with the same temporal frequency but different mode order  $n'$  (D’Silva 1994; Fan et al. 1995). Since flux tubes in the solar atmosphere flare with height (a consequence of the pressure stratification), mode mixing certainly occurs. To what extent, however, is still unclear. This uncertainty is further complicated when one considers the existence of the *acoustic jacket*. Bogdan & Cally (1995) demonstrated that a continuous spectrum of laterally evanescent surface waves is necessary to satisfy boundary conditions at the sunspot interface. These “jacket modes” are excited by incident acoustic waves and are capable of carrying away energy along the field lines.

Here, we examine an additional source of absorption that may operate in plage regions where the field is composed of a collection of thin fibrils. As suggested in Bogdan et al. (1996) (hereinafter called BHCC1996) and in Hindman & Jain (2008) (subsequently referred to as HJ2008), we consider the following mechanism: within the solar convection zone  $p$ -mode oscillations pummel the many magnetic fibrils that comprise the plage. This buffeting excites both longitudinal sausage waves and transverse kink waves which then carry energy up and down the fibrils. Those waves that travel downward are lost in the convection zone, whereas those that propagate upward pass through the photosphere into the upper atmosphere where they manifest as coronal-loop oscillations and upward-propagating waves. In either case, the energy is extracted from the  $p$  modes and removed from the acoustic cavity.

In this paper, we calculate—by a semianalytic method—the absorption coefficient, which is a measure of the difference between the ingoing and outgoing  $p$ -mode power. For our model, there is more ingoing  $p$ -mode power due to the conversion of acoustic energy into magnetic tube waves. Our present calculations are a direct extension of the work carried out in HJ2008 where we demonstrated that  $f$  and  $p$  modes efficiently generate tube waves and that an energy flux in excess of

$10^5 \text{ erg cm}^{-2} \text{ s}^{-1}$  can be driven upward through photospheric levels. This energy sink for  $f$  and  $p$  modes depends on the boundary condition applied at the model photosphere and on the temporal frequency of the incident wave.

The paper is organized as follows: the derivation of the first-order scattering equations is presented in Section 2. In Section 3, we detail the equilibrium atmosphere and the model flux tube. Section 4 describes the governing equations for the  $p$ -mode oscillations and the driven tube waves. Section 5 provides a calculation of the absorption coefficient. In Section 6, we present our results and in Section 7, we discuss our findings, including a comparison of our derived absorption coefficients with those obtained by observations.

## 2. WEAK FIRST-ORDER SCATTERING

If we assume that we have an isolated, compact region of magnetic field embedded within a nonmagnetized atmosphere, we can express the total wave function in the field-free region as the sum of three components,

$$\Phi(\mathbf{x}, t) = \Phi_{\text{inc}}(\mathbf{x}, t) + \Phi_{\text{sc}}(\mathbf{x}, t) + \Phi_{\text{jac}}(\mathbf{x}, t). \quad (1)$$

Here  $\Phi$  can be any wave variable we might care to consider. For example, later in this paper we will define  $\Phi$  as the displacement potential.  $\Phi_{\text{inc}}$  is the unperturbed  $p$ -mode wave field that would exist in the absence of the magnetic flux concentration (i.e., the incident wave field).  $\Phi_{\text{sc}}$  represents a discrete set of propagating scattered waves in the form of outgoing  $p$  modes.  $\Phi_{\text{jac}}$  is the contribution due to the continuous spectrum of laterally evanescent jacket modes (see Bogdan & Cally 1995). We can express an arbitrary wave field of incident  $p$  modes as a Fourier–Bessel decomposition in cylindrical polar coordinates,  $\mathbf{x} = (r, \phi, z)$ , where the origin is centered on the flux concentration,

$$\Phi_{\text{inc}}(r, \phi, z, \omega) = \sum_{m=-\infty}^{\infty} \sum_{n=0}^{\infty} \mathcal{A}_{mn}(\omega) e^{im\phi} J_m(k_n r) Q_n(z). \quad (2)$$

In this expression—and in the subsequent two—we have chosen to apply temporal Fourier transforms ( $t \rightarrow \omega$ ) and to work in frequency space. The coefficients  $\mathcal{A}_{mn}(\omega)$  are arbitrary complex amplitudes that characterize the incident wave field,  $J_m(k_n r)$  is the Bessel function of the first kind,  $Q_n(z)$  is the vertical eigenfunction for the  $n$ th-order  $p$  mode, and  $k_n = k_n(\omega)$  is the wavenumber eigenvalue for the  $n$ th-order  $p$  mode with frequency  $\omega$ .

Using similar expansions, the scattering terms become

$$\begin{aligned} \Phi_{\text{sc}}(r, \phi, z, \omega) = & \sum_{m=-\infty}^{\infty} \sum_{n=0}^{\infty} \mathcal{A}_{mn}(\omega) e^{im\phi} \\ & \times \sum_{n'=0}^{\infty} S_m^{n \rightarrow n'}(\omega) H_m^{(1)}(k_{n'} r) Q_{n'}(z), \quad (3) \end{aligned}$$

$$\begin{aligned} \Phi_{\text{jac}}(r, \phi, z, \omega) = & \sum_{m=-\infty}^{\infty} \sum_{n=0}^{\infty} \mathcal{A}_{mn}(\omega) e^{im\phi} \\ & \times \int_0^{\infty} d\Lambda T_m^{n \rightarrow \Lambda}(\omega) K_m(\Lambda r) q(\Lambda; z). \quad (4) \end{aligned}$$

Here  $H_m^{(1)}(k_n r)$  is the Hankel function of the first kind and  $K_m(\Lambda r)$  is the modified Bessel function of the second kind with  $\Lambda^{-1}$  being the lateral decay length for the jacket modes. There are two separate scattering matrices:  $S_m^{n \rightarrow n'}$  represents scattering into outgoing propagating  $p$  modes, whereas  $T_m^{n \rightarrow \Lambda}$  represents the excitation of the acoustic jacket. The functions  $q(\Lambda; z)$  describe the vertical behavior of each jacket mode and are generally oscillatory with depth. Note that when  $S_m^{n \rightarrow n'}$  is nonzero for  $n \neq n'$ , mode mixing is occurring where an incoming  $p$  mode of order  $n$  is scattered into an outgoing  $p$  mode of order  $n'$ .

In general, the two scattering matrices,  $S_m^{n \rightarrow n'}$  and  $T_m^{n \rightarrow \Lambda}(\omega)$ , tell us everything we need to know about the wave–tube interaction, including the absorption coefficient and phase shift. Observationally, the absorption coefficient has traditionally been defined as the ratio of the difference between the ingoing and outgoing power to the ingoing power at the same frequency  $\omega$ , mode order  $n$ , and azimuthal order  $m$ ,

$$\alpha_{mn}(\omega) \equiv 1 - |1 + 2S_m^{n \rightarrow n}(\omega)|^2. \quad (5)$$

This definition (e.g., Braun 1995) ignores the existence of mode mixing and the excitation of the acoustic jacket. This assumption is assuredly incorrect, but for simplicity and in order to estimate the relative contribution of energy absorption, mode mixing and jacket excitation, we adopt a systematic approach where we examine each effect in isolation. Similar calculations by Hanasoge et al. (2008), where they examined the excitation of kink waves by an incident  $f$  mode, seem to indicate that the mode mixing is weak for thin flux tubes. In the current paper, we will only consider absorption of acoustic waves arising from the excitation of magnetic tube waves. Mode mixing and the acoustic jacket will be left to subsequent work.

## 3. THE MODEL

We investigate the interaction between acoustic waves and magnetic fibrils beneath the solar photosphere. The fibril field is assumed to consist of an ensemble of untwisted, axisymmetric, thin flux tubes embedded inside a polytropically stratified field-free atmosphere. This model was discussed in detail in HJ2008, but we describe it here briefly to aid the reader's understanding.

### 3.1. The Nonmagnetic Interior

We model the solar convection zone with a plane-parallel atmosphere with uniform gravity acting in the downward direction  $\mathbf{g} = -g\hat{\mathbf{z}}$ , with the height  $z$  increasing upward. The atmosphere is polytropic below the height  $z < -z_0$ , which corresponds to the model's photosphere. The gas pressure, mass density and sound speed vary with  $z$  as power laws,

$$\begin{aligned} P_{\text{ext}}(z) &= \frac{gz_0 \rho_0}{a+1} \left(-\frac{z}{z_0}\right)^{a+1} = P_0 \left(-\frac{z}{z_0}\right)^{a+1}, \\ \rho_{\text{ext}}(z) &= \rho_0 \left(-\frac{z}{z_0}\right)^a, \quad c_{\text{ext}}^2(z) = -\frac{gz}{a}. \end{aligned}$$

The quantities  $\rho_0$  and  $P_0$  are the values of the mass density and gas pressure at the photosphere  $z = -z_0$ . The value of the polytropic index  $a$  is set such that the stratification is neutrally stable to buoyancy; this requires  $a = 1/(\gamma - 1)$ , where  $\gamma$  is the ratio of specific heats. Above  $z = -z_0$ , we assume the existence of a hot vacuum ( $\rho_{\text{ext}} \rightarrow 0$  with temperature  $T_{\text{ext}} \rightarrow \infty$ ), with

the property that the gas pressure ( $P_{\text{ext}} \sim \rho_{\text{ext}} T_{\text{ext}}$ ) is finite and continuous across the  $z = -z_0$  layer. Note, in the notation of HJ2008, the polytropic index was denoted with the letter  $m$ . However, to avoid confusion with the azimuthal order, we have used the variable  $a$  here instead.

Following BHCC1996 and HJ2008, we specify the depth of the photosphere  $z_0$  and the surface mass density  $\rho_0$  (and therefore the surface pressure  $P_0$ ) by matching our model photosphere to the  $\tau_{5000} = 1$  level of a solar model by Maltby et al. (1986). At this layer in the solar model  $g = 2.775 \times 10^4 \text{ cm s}^{-1}$ ,  $\rho_0 = 2.78 \times 10^{-7} \text{ g cm}^{-3}$ , and  $P_0 = 1.21 \times 10^5 \text{ g cm}^{-1} \text{ s}^{-1}$ . We will use polytropic index  $a = 1.5$  for our calculations.

### 3.2. The Magnetic Flux Tubes

We assume that the magnetic fibrils threading this field-free atmosphere are untwisted, straight, vertically aligned, thin tubes with a circular cross section. By the term *thin*, we mean that all the characteristic scale lengths—such as the wavelength of the acoustic oscillations and the density scale height—are much larger than the radius of the tube. Such a thin flux tube, although in hydrostatic balance, is unable to support internal lateral structure and hence the temperature and total pressure will be uniform across the tube and continuous with their external values. Since the total pressure, therefore, has the same scale height inside and outside the tube, the magnetic pressure inside the tube has the same scale height as the gas pressure. This mandates that the plasma parameter  $\beta$ , defined as the ratio of gas pressure to the magnetic pressure, is constant with height inside the tube. Since we only consider tubes below the photosphere (i.e.,  $z < -z_0$ ), we need not worry about the rapid flaring of tubes into a magnetic canopy that occurs within the chromosphere.

We ignore lateral variation of the magnetic field strength and describe the tube's internal gas pressure  $P(z)$ , mass density  $\rho(z)$ , and field strength  $B(z)$  by their axial values. These three quantities as well as the tube's cross-sectional area  $A(z)$  can be described uniquely by the total magnetic flux contained by the tube  $\Theta$  and the plasma  $\beta$ ,

$$P(z) = \frac{\beta}{\beta + 1} P_{\text{ext}}(z), \quad \rho(z) = \frac{\beta}{\beta + 1} \rho_{\text{ext}}(z),$$

$$\frac{B^2(z)}{8\pi} = \frac{1}{\beta + 1} P_{\text{ext}}(z), \quad A(z) = \frac{\Theta}{B(z)} = \left( \frac{\beta + 1}{8\pi P_{\text{ext}}(z)} \right)^{1/2} \Theta.$$

For a flux tube with  $\beta = 1$  embedded in a polytropic atmosphere with  $a = 1.5$  and with a surface mass density of  $\rho_0 = 2.78 \times 10^{-7} \text{ g cm}^{-3}$ , the magnetic field strength at the photosphere,  $z = -z_0$ , is  $B_0 = 1.2 \text{ kG}$ .

## 4. THE GOVERNING WAVE EQUATIONS

The field-free medium supports acoustic oscillations (the  $f$  and  $p$  modes), while thin flux tubes permit the propagation of both longitudinal (sausage) and transverse (kink) MHD waves. Note, thin flux tubes can also support torsional Alfvén waves; however, we ignore such waves, because the  $p$  modes are irrotational in our model and do not couple to torsional modes. In the following subsections, we briefly present the governing equations for these waves and describe the driving of the tube waves by the acoustic waves.

### 4.1. The $f$ and $p$ Modes

For the atmosphere described here, it is easy to demonstrate that if  $\Phi$  is the displacement potential, the vertical eigenfunction  $Q_n(z)$  that appears in Equations (2) and (3) is proportional to Whittaker's  $W$  function (Abramowitz & Stegun 1964, p. 507; see BHCC1996 or HJ2008 for a complete derivation),

$$Q_n(z) = w^{-(\mu+1/2)} W_{\kappa_n, \mu}(w), \quad (6)$$

where  $w = -2k_n z$  is a dimensionless depth and

$$\mu \equiv (a + 1)/2, \quad v^2 \equiv \frac{a\omega^2 z_0}{g}, \quad \kappa_n \equiv \frac{v^2}{2k_n z_0}.$$

The quantization of the horizontal wavenumber  $k_n$  (or equivalently  $\kappa_n$ ) arises from the requirement that the Lagrangian pressure perturbation vanish at the model photosphere. Mathematically, this takes the form

$$W_{\kappa_n, \mu+1}(\lambda_n) = 0, \quad (7)$$

where  $\lambda_n = 2k_n z_0$  is a dimensionless photospheric depth.

In a subsequent calculation, we will need to know the lateral energy flux carried by a  $p$  mode. We have expressed our  $p$  modes in cylindrical geometry,

$$\Phi_{mn}(r, \phi, z, \omega) = e^{im\phi} H_m^{(1 \text{ or } 2)}(k_n r) Q_n(z), \quad (8)$$

where the Hankel function of the first kind is used for waves propagating outward, away from the flux tube. The Hankel function of the second kind is used for waves propagating inward. Once integrated in azimuth, the lateral energy flux of such waves is purely horizontal, either toward or away from the axis of coordinates where the flux tube resides. The lateral energy flux carried by any individual wave component, can be obtained by averaging the product of the perturbed pressure  $\delta P$  and the radial velocity  $v_r$  in time, followed by integration over a vertical cylinder of radius  $r$ ,

$$F = \frac{1}{4} \int_0^{2\pi} r d\phi \int_{-\infty}^{-z_0} dz (\delta P v_r^* + \delta P^* v_r), \quad (9)$$

where the \* denotes complex conjugation.

If we utilize  $\mathbf{v} = -i\omega \nabla \Phi$  and  $\delta P = \rho \omega^2 \Phi$ , the horizontal energy flux for an outward propagating wave can be reduced to

$$F_n \equiv 2 \frac{\rho_0}{z_0^{1/2}} \left( \frac{g}{a} \right)^{3/2} \frac{v^3}{\lambda_n^{a+1}} \mathcal{H}_n, \quad (10)$$

where

$$\mathcal{H}_n \equiv \int_{\lambda_n}^{\infty} dw w^a Q_n^2(w). \quad (11)$$

We have adopted the convention that the sign of an outward energy flux is positive. The energy flux for the inward propagating wave component is simply the negative of the result in Equation (10).

### 4.2. The Tube Waves

Thin flux tubes support both longitudinal (sausage) waves and transverse (kink) waves. Here, these oscillations are driven by the agitation of the tube by external  $f$ - and  $p$ -mode oscillations.

Using the formulation of HJ2008, the fluid displacement within the tube can be described by the following equations:

$$\left\{ \frac{\partial^2}{\partial t^2} - c_T^2 \frac{\partial^2}{\partial z^2} + \frac{\gamma g}{2} \frac{c_T^2}{c^2} \frac{\partial}{\partial z} \right\} \xi_{\parallel} = \frac{\rho_{\text{ext}}}{\rho} \frac{c_T^2}{V_A^2} \left. \frac{\partial^3 \Phi_{\text{inc}}}{\partial z \partial t^2} \right|_{r=0}, \tag{12}$$

$$\left\{ \frac{\partial^2}{\partial t^2} - c_K^2 \frac{\partial^2}{\partial z^2} + \frac{\gamma g}{2} \frac{c_K^2}{c^2} \frac{\partial}{\partial z} \right\} \xi_{\perp} = 2 \frac{\rho_{\text{ext}}}{\rho} \frac{c_K^2}{V_A^2} \left. \frac{\partial^2 \nabla \Phi_{\text{inc}}}{\partial t^2} \right|_{r=0}, \tag{13}$$

where  $V_A$  is the Alfvén speed,  $c_T$  is the cusp or tube speed and  $c_K$  is the kink speed,

$$V_A^2 = \frac{B^2}{4\pi\rho}, \quad c_T^2 = \frac{c^2 V_A^2}{c^2 + V_A^2}, \quad c_K^2 = \frac{B^2}{4\pi(\rho + \rho_{\text{ext}})}.$$

In Equations (12) and (13),  $\xi_{\parallel}$  indicates the vertical displacement resulting from sausage waves and  $\xi_{\perp}$  applies to the horizontal displacement from kink waves. The terms on the right-hand side of each equation are due to the forcing by the incident wave and are evaluated at  $r = 0$  along the flux tube’s axis. We have implicitly adopted the Born approximation, by assuming that the driving terms only depend on the incident wave field, ignoring the scattered field and the acoustic jacket.

The forcing provided by each individual incident  $p$  mode can be obtained by evaluating the expression for the incident wave field, Equation (2), at  $r = 0$  and inserting the result into these two wave equations. After Fourier transforming in time  $t$ , one obtains

$$\left\{ c_T^2 \frac{\partial^2}{\partial z^2} - \frac{\gamma g}{2} \frac{c_T^2}{c^2} \frac{\partial}{\partial z} + \omega^2 \right\} \xi_{\parallel} = \frac{\rho_{\text{ext}}}{\rho} \frac{c_T^2}{V_A^2} \omega^2 \sum_{n=0}^{\infty} \mathcal{A}_{0,n}(\omega) \frac{dQ_n(z)}{dz}, \tag{14}$$

$$\left\{ c_K^2 \frac{\partial^2}{\partial z^2} - \frac{\gamma g}{2} \frac{c_K^2}{c^2} \frac{\partial}{\partial z} + \omega^2 \right\} \xi_{\perp} = 2 \frac{\rho_{\text{ext}}}{\rho} \frac{c_K^2}{V_A^2} \omega^2 \sum_{n=0}^{\infty} ik_n \Upsilon_n(\omega) Q_n(z), \tag{15}$$

where

$$\Upsilon_n(\omega) = \frac{i}{2} [\mathcal{A}_{-1,n}(\omega) - \mathcal{A}_{1,n}(\omega)] \hat{x} + \frac{1}{2} [\mathcal{A}_{-1,n}(\omega) + \mathcal{A}_{1,n}(\omega)] \hat{y}. \tag{16}$$

Note that only the  $p$  modes with  $m = 0$  contribute to the forcing of the sausage waves and only the  $|m| = 1$  modes drive kink waves. All other azimuthal components vanish in the limit  $r \rightarrow 0$ .

In HJ2008, it was found that sufficiently below the lower turning point of the  $p$  mode driving the tube waves, the rate at which energy passes down the tube is constant with depth,

$$\dot{E}_{\parallel}^{(d)} = - \frac{\gamma\beta}{2 + \gamma\beta} \frac{\pi g \rho_0 \omega A_0}{4(a+1)(\beta+1)} \frac{|\mathcal{A}_{0,n}|^2}{z_0^2} |\Omega_{\parallel} + \mathcal{I}_{\parallel}^*|^2, \tag{17}$$

$$\dot{E}_{\perp}^{(d)} = - \frac{\pi g \rho_0 \omega A_0}{4(a+1)(\beta+1)} \frac{|\Upsilon_n|^2}{z_0^2} |\Omega_{\perp} - \mathcal{I}_{\perp}^*|^2, \tag{18}$$

where the leading negative sign indicates downward energy flux, or energy escaping the  $p$ -mode cavity, and the superscript (d) refers to the downward flux. These energy fluxes are the fluxes driven by a single  $p$  mode of order  $n$ . Also,  $A_0$  is the cross-sectional area of the tube at the photosphere (not to be confused with  $\mathcal{A}_{mn}$ ),  $\mathcal{I}_{\parallel}$  and  $\mathcal{I}_{\perp}$  are the interaction integrals between the  $p$  mode and the respective tube wave, and  $\Omega_{\parallel}$  and  $\Omega_{\perp}$  are parameters that specify the boundary condition applied at the model photosphere (see HJ2008 for the details of these parameters). The interaction integrals are integrations in depth over the entire length of the tube and the integrands are the product of the free oscillations of the tube and the  $p$ -mode driving, the right-hand sides of Equations (14) and (15). The boundary condition parameters can satisfy any physical choice of boundary condition with a suitable assignment of values.

A similar result can be obtained at the model photosphere,

$$\dot{E}_{\parallel}^{(u)} = - \frac{\gamma\beta}{2 + \gamma\beta} \frac{\pi g \rho_0 \omega A_0}{4(a+1)(\beta+1)} \frac{|\mathcal{A}_{0,n}|^2}{z_0^2} (|\mathcal{I}_{\parallel}|^2 - |\Omega_{\parallel}|^2 + \mathcal{S}), \tag{19}$$

$$\dot{E}_{\perp}^{(u)} = - \frac{\pi g \rho_0 \omega A_0}{4(a+1)(\beta+1)} \frac{|\Upsilon_n|^2}{z_0^2} (|\mathcal{I}_{\perp}|^2 - |\Omega_{\perp}|^2). \tag{20}$$

Here, the  $\mathcal{S}$  term, which arises due to the nonvanishing driver at the surface, is the product of the  $p$ -mode eigenfunction and the real part of the vertical displacement (see HJ2008 for a full definition). The negative sign in the above equations once again indicates energy escaping the  $p$ -mode cavity and the superscript (u) refers to the upward flux.

### 5. THE ABSORPTION COEFFICIENT FOR A SINGLE TUBE

Since we are ignoring the effects of mode mixing and jacket modes, Equation (1) can be expanded using only a subset of terms,

$$\Phi(r, \phi, z, \omega) = \sum_{m=-\infty}^{\infty} \sum_{n=0}^{\infty} \frac{\mathcal{A}_{mn}(\omega)}{2} e^{im\phi} Q_n(z) \times [H_m^{(2)}(k_n r) + (1 + 2S_m^{n \rightarrow n}(\omega)) H_m^{(1)}(k_n r)]. \tag{21}$$

Here, we have used the fundamental relation  $J_m = (H_m^{(1)} + H_m^{(2)})/2$ . The first term in the braces (with the Hankel function of the second kind) corresponds to the inward propagating portion of the incident wave field. The second term (with the Hankel function of the first kind) contains the contributions from both the outward propagating component of the unperturbed wave and the outgoing scattered wave.

Using Equation (5), we can replace the diagonal elements of the scattering matrix that appear in Equation (21) with the absorption coefficient,

$$\Phi(r, \phi, z, \omega) = \sum_{m=-\infty}^{\infty} \sum_{n=0}^{\infty} \frac{\mathcal{A}_{mn}(\omega)}{2} e^{im\phi} Q_n(z) \times [H_m^{(2)}(k_n r) + \sqrt{1 - \alpha_{mn}} H_m^{(1)}(k_n r)]. \tag{22}$$

Since the tube is axisymmetric, only the  $m = 0$  component of the unperturbed solution generates sausage modes and scatters into  $m = 0$  waves, and a similar statement holds between the  $m = \pm 1$  components and kink waves. Thus, conservation of energy requires that the deficit of power between ingoing and outgoing waves with  $m = 0$  is equal to the rate that sausage waves remove energy from the  $p$ -mode cavity, while the deficit for waves with  $m = \pm 1$  is given by the rate for kink waves. Using these conservation of energy arguments, one may write

$$\dot{E}_{\parallel} \equiv \dot{E}_{\parallel}^{(d)} + \dot{E}_{\parallel}^{(u)} = -\frac{F_n}{4} |\mathcal{A}_{0,n}|^2 \alpha_{0,n}, \quad (23)$$

$$\begin{aligned} \dot{E}_{\perp} &\equiv \dot{E}_{\perp}^{(d)} + \dot{E}_{\perp}^{(u)} = -\frac{F_n}{4} (|\mathcal{A}_{-1,n}|^2 \alpha_{-1,n} + |\mathcal{A}_{1,n}|^2 \alpha_{1,n}) \\ &= -\frac{F_n}{4} (|\mathcal{A}_{-1,n}|^2 + |\mathcal{A}_{1,n}|^2) \alpha_{1,n} \\ &= -\frac{F_n}{2} |\Upsilon_n|^2 \alpha_{1,n}, \end{aligned} \quad (24)$$

where we have used the lateral energy flux for the propagating  $p$  modes, Equation (10), to express the rate at which energy is carried toward and away from the axis of coordinates where the flux tube resides. Furthermore, we have exploited the fact that  $\alpha_{-1,n} = \alpha_{1,n}$ .

We insert Equations (10) and (17)–(20) into the two previous Equations (23) and (24), to find an expression for the absorption coefficient as a function of the interaction integrals and boundary condition parameters,

$$\begin{aligned} \alpha_{0,n} &= \frac{\pi \beta}{2(2 + \gamma \beta)(\beta + 1)} \frac{\lambda_n^{a+1}}{v^2 \mathcal{H}_n} \frac{A_0}{z_0^2} \\ &\quad \times (|\Omega_{\parallel} + \mathcal{I}_{\parallel}^*|^2 + |\mathcal{I}_{\parallel}|^2 - |\Omega_{\parallel}|^2 + \mathcal{S}), \end{aligned} \quad (25)$$

$$\alpha_{\pm 1,n} = \frac{\pi}{4\gamma(\beta + 1)} \frac{\lambda_n^{a+1}}{v^2 \mathcal{H}_n} \frac{A_0}{z_0^2} (|\Omega_{\perp} - \mathcal{I}_{\perp}^*|^2 + |\mathcal{I}_{\perp}|^2 - |\Omega_{\perp}|^2). \quad (26)$$

In order to use these expressions to compute the absorption coefficients, we must first specify the boundary condition that will be applied to the tube waves at the photosphere. In HJ2008, we presented results derived by applying two different boundary conditions. The first of these required the stress to vanish at the photosphere; thus, the energy flux through the upper surface is identically zero. The second boundary condition requires minimum reflection at the upper surface. In other words, this boundary condition allows the maximum energy flux of tube waves to be driven into the upper atmosphere.

We demonstrated in HJ2008 that the stress-free boundary produces significant damping of the  $f$  mode through the excitation of tube waves. Most of the energy is converted into kink waves. Conversely, the maximal-flux boundary converts more acoustic energy into sausage waves and the resulting damping is important for  $n < 5$ . For both boundary conditions the damping vanishes at zero frequency and rises rapidly as the frequency increases. We expect similar functional dependences for the absorption coefficients.

We now present, as Figures 1–3, the absorption coefficient computed for both of these boundary conditions and for three

different values of  $\beta$  (0.1, 1.0, and 10.0). We assume that the polytropic index is  $a = 1.5$  and that the photospheric radius of the tube is  $R_0 = 0.1$  Mm. For the maximal-flux boundary condition, the absorption coefficient due to the excitation of sausage waves increases with increasing  $\beta$ , whereas it decreases slightly with increasing  $\beta$  for the kink waves. For the stress-free boundary condition the behavior is not monotonic due to the existence of frequencies for which the downward propagating wave, generated directly by the driver, destructively interferes with the wave reflected off of the stress-free upper boundary. This is identical to the behavior that was seen in HJ2008 for the damping rates.

There are two competing effects at play. As  $\beta$  increases and the photospheric field strength decreases, the flux tube increases in cross-sectional area in order to maintain the same magnetic flux ( $A_0 \sim \sqrt{1 + \beta}$ ). This tends to increase the energy flux carried by the tube purely by increasing the surface area over which energy can be transmitted. The second effect is a change in the excitation itself. Maximal excitation arises when the wavelength of the tube wave is comparable to the vertical wavelength of the driving  $p$  mode. Since, both wavelengths are nonuniform with height and have different height profiles, no direct wavelength matching is possible. However, as the value of  $\beta$  increases, the tube wave rapidly becomes much shorter in wavelength and the excitation becomes less efficient. Thus eventually, for sufficiently high  $\beta$ , the excitation diminishes. The wavelengths of the kink waves are, in general, shorter than the wavelengths of the sausage waves at the same frequency. This means that the value of  $\beta$  for which driving becomes less efficient is less for the kink mode than the sausage mode. For the frequency regime covered here, the kink waves fall into the weak excitation regime for moderate values of  $\beta$ , hence the observed decrease in the absorption coefficient as  $\beta$  increases. The sausage mode, however, has not yet entered this weak excitation regime.

Note that in Figure 1, the absorption coefficients arising from the excitation of kink waves for the case of the stress-free photospheric boundary has nulls where the absorption coefficient vanishes. These nulls are expected due to the destructive interference between the wave reflected from the photosphere back into convection zone and the downward propagating wave directly generated by the driver (see also HJ2008). If we extend the curves to much higher (and unobserved) frequencies, all of the absorption curves for the stress-free boundary would display such nulls.

## 6. THE ABSORPTION COEFFICIENT FOR PLAGE

In the following section, we will attempt to apply our theoretical results to model the absorption coefficient for solar plage. In particular, we will model the plage observed by Braun & Birch (2008) using the helioseismic technique of ridge-filtered holography. Braun & Birch (2008) have produced maps of the absorption coefficient for different wave frequencies and mode orders. These maps span a  $60^\circ \times 60^\circ$  region of the solar surface and were obtained using Michelson Doppler Imager (MDI) data taken over a period of time lasting 27 hr and starting on 2002 April 1.

Equations (25) and (26) are the absorption coefficient for a single, thin flux tube. We will model a plage by examining the effect of a large number of identical thin flux tubes. We assume that the tubes are sufficiently distant from each other that they do not sit within each others' acoustic jackets and that we can describe the absorption using the first-order Born approximation

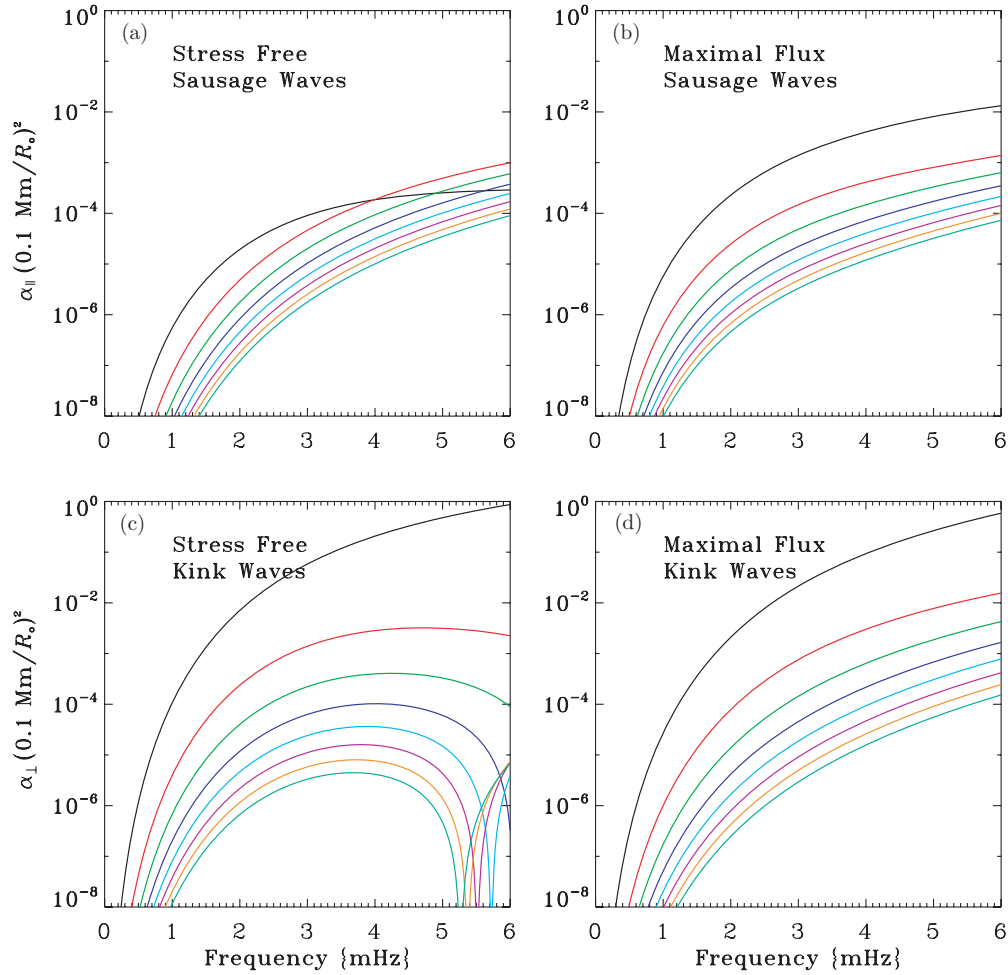


**Figure 1.** Absorption coefficient as a function of frequency for a single, thin flux tube with a plasma  $\beta = 0.1$ , embedded in a polytropic atmosphere with an index  $a = 1.5$ . Each mode order is plotted with a different color: black ( $f$ ), red ( $p_1$ ), green ( $p_2$ ), etc. For the kink modes, the sum of the absorption coefficient over  $m = -1$  and  $m = 1$  is shown.

(A color version of this figure is available in the online journal.)

(which is consistent with our method for calculating the tube wave excitation). For such an ensemble of tubes, we may estimate their collective absorption coefficient by multiplying the absorption coefficient for a single tube by the number of tubes  $N$  in the ensemble,

$$\alpha_{\parallel,n} = \alpha_{0,n}N, \quad (27)$$

$$\alpha_{\perp,n} = (\alpha_{-1,n} + \alpha_{1,n})N, \quad (28)$$

where  $\alpha_{\parallel,n}$  is the plane's absorption coefficient for waves with  $m = 0$  and  $\alpha_{\perp,n}$  is the absorption coefficient for the sum of the  $m = -1$  and  $m = 1$  waves.

We have previously calculated  $\alpha_{m,n}$ ; therefore, the only remaining unknown ingredient is the appropriate number of tubes to include. Effectively, we need to estimate how many magnetic flux tubes a measurement samples at any given point in the absorption map. Within the Born approximation, the measurement at a single point in the map is actually a spatially weighted average of the magnetic flux within an extended region around that point. The spatial weighting function,  $K_n$ , is called the averaging kernel and is a function of both the radial order of the mode and the frequency. Since the kernel linearly relates the

absorption coefficient to the distribution of magnetic flux, the number of tubes in the ensemble is equal to the magnetic flux sampled by the kernel,  $\Theta_n(\omega)$ , divided by the magnetic flux of an individual tube,  $\Theta = B_0A_0$ ,

$$N = \frac{\Theta_n(\mathbf{r}, \omega)}{B_0A_0}, \quad (29)$$

$$\Theta_n(\mathbf{r}, \omega) \equiv \int d\mathbf{r}' K_n(\mathbf{r}' - \mathbf{r}, \omega) |B(\mathbf{r}')|, \quad (30)$$

where  $|B|$  is the modulus of the photospheric magnetic field as a function of position,  $\mathbf{r}$  is the observation point in the absorption map, and  $\mathbf{r}'$  is any other point on the solar surface.

The kernel's spatial form depends largely on the wavelength of the acoustic waves used by the measurement, but may also depend on details of the observational scheme. At present, the exact form of the averaging kernel is unknown for this set of observations; however, prior experience dictates that the kernel is peaked near the observation point  $\mathbf{r}$  and decays with distance from that point with a width roughly equal to the horizontal wavelength of the acoustic waves. For this study, we make the reasonable assumption that the kernel is Gaussian in profile

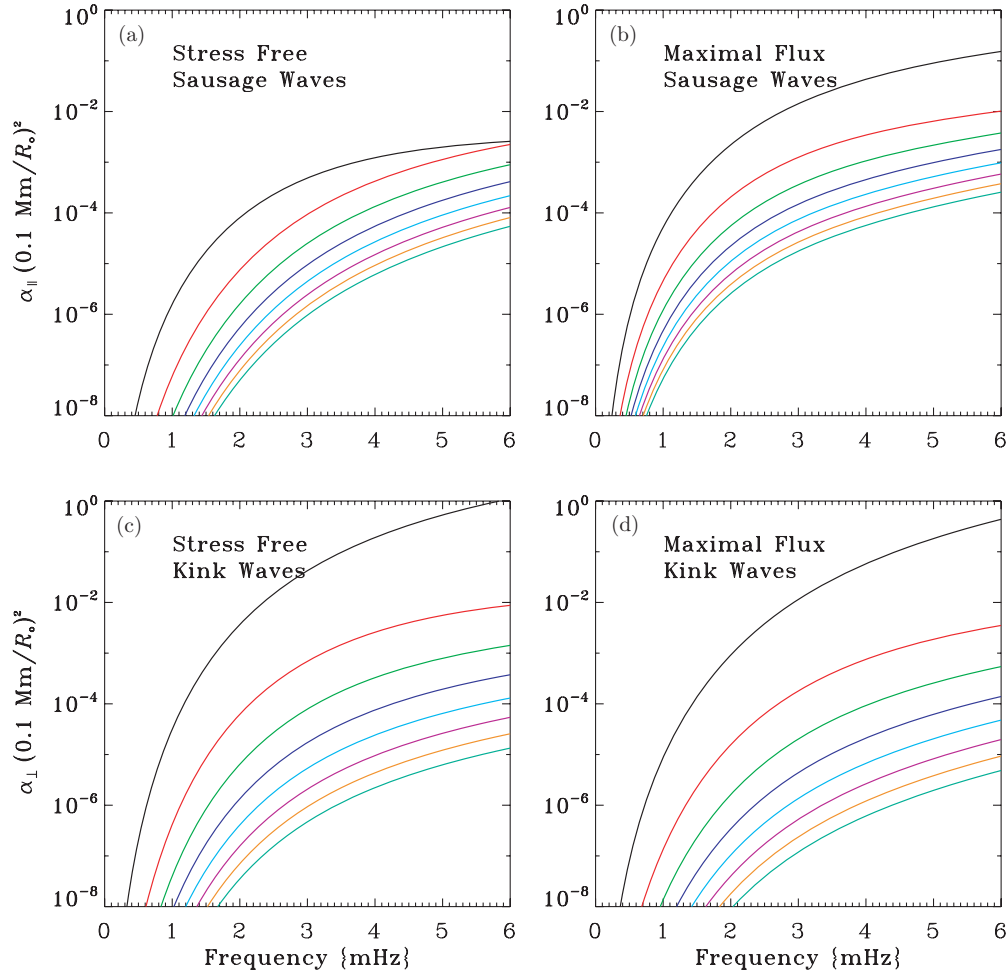


**Figure 2.** The same as Figure 1 except that the thin flux tube has  $\beta = 1$ .  
(A color version of this figure is available in the online journal.)

with a width equal to the horizontal wavelength of the primary  $p$  modes involved in the measurement,

$$K_n(\mathbf{r}, \omega) = \exp\left(-\frac{k_n^2 |\mathbf{r}|^2}{\pi^2}\right). \quad (31)$$

We have tested a variety of kernel profiles, including a top hat function in radius, and the results that follow are rather insensitive to the specific profile used as long as the kernel possesses the same integrated area  $A_{\text{kern}}$ ,

$$A_{\text{kern}} = \int d\mathbf{r} K_n(\mathbf{r}, \omega) = \frac{\pi^3}{k_n^2}. \quad (32)$$

In the definition of  $\Theta_n$  in Equation (30), we estimate  $|B|$  using MDI magnetograms. Figure 4(a) shows a magnetogram for an area that spans  $60^\circ \times 60^\circ$  on the solar surface. This is the same region analyzed by Braun & Birch (2008). Figures 4(b)–(d) show  $\Theta_n(\mathbf{r}, \omega)$  for three kernels with different frequencies, 2.0 mHz, 3.5 mHz, and 5.0 mHz, respectively.

A more easily interpreted quantity is the mean field strength sampled by the kernel,

$$B_n(\mathbf{r}, \omega) = \frac{\Theta_n(\mathbf{r}, \omega)}{A_{\text{kern}}}. \quad (33)$$

$B_n$  can be interpreted as the field strength smoothed by convolution with the kernel. To assess the relative size of  $B_n$  we

average  $B_n$  over all pixels within the magnetogram associated with the plage. We use the same definition of plage as Braun & Birch (2008). Umbra and penumbra are rejected by eliminating all pixels whose brightness falls below 92% of the mean MDI continuum values. Of the remaining pixels, those with a field strength greater than 100 G are identified as plage. Figure 5 shows the result of this averaging. The mean field strength is roughly 200 G at high frequencies and falls at low frequencies by 10%–25%, depending on the mode order. Low frequencies and high mode orders have longer horizontal wavelengths; therefore, the kernels formed from such waves sample a larger spatial area. Thus, at low frequencies and high mode orders, a significant fraction of the kernel area contains quiet Sun resulting in a reduction in the mean field strength.

By combining Equations (25) and (26) with Equations (32) and (33) we obtain an estimate for the absorption that should be measured for the plage,

$$\alpha_{\parallel,n} = \frac{2\pi^4 \beta}{(2 + \gamma\beta)(\beta + 1)} \frac{\lambda_n^{\alpha-1}}{v^2} \frac{B_n}{B_0} \frac{|\Omega_{\parallel} + \mathcal{I}_{\parallel}^*|^2 + |\mathcal{I}_{\parallel}|^2 - |\Omega_{\parallel}|^2 + \mathcal{S}}{\mathcal{H}_n}, \quad (34)$$

$$\alpha_{\perp,n} = \frac{2\pi^4}{\gamma(\beta + 1)} \frac{\lambda_n^{\alpha-1}}{v^2} \frac{B_n}{B_0} \frac{|\Omega_{\perp} - \mathcal{I}_{\perp}^*|^2 + |\mathcal{I}_{\perp}|^2 - |\Omega_{\perp}|^2}{\mathcal{H}_n}, \quad (35)$$

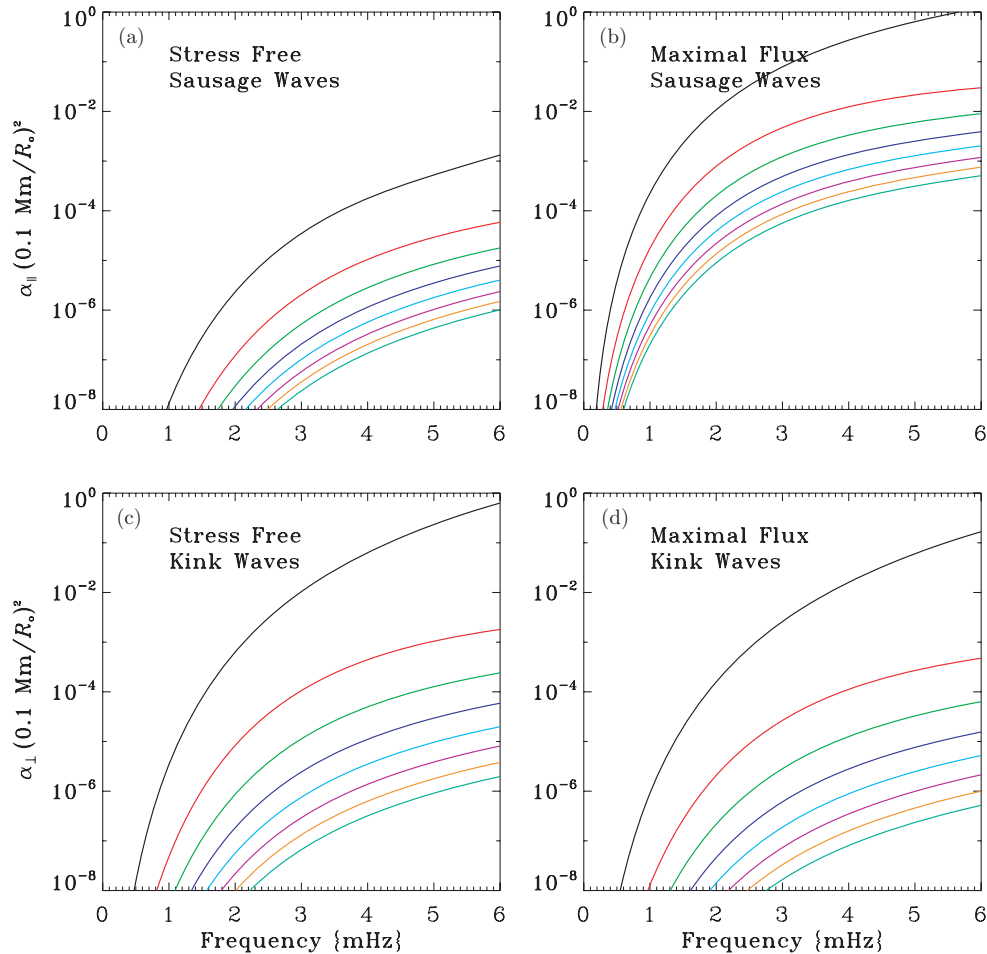


**Figure 3.** The same as Figures 1 and 2 except for  $\beta = 10$ .  
(A color version of this figure is available in the online journal.)

where  $\alpha_{\perp,n}$  is the absorption coefficient for the sum of the  $m = -1$  and  $m = 1$  modes.

Figure 6 presents the absorption coefficients that we obtain for our model plage, using Equations (34) and (35) and the mean field strengths shown in Figure 5. The absorption for  $m = 0$  (due to excitation of sausage waves) and for  $|m| = 1$  (due to excitation of kink waves) is plotted as solid and dashed curves respectively for  $p_1$  through  $p_4$ . We have shown only  $p_1$  through  $p_4$  because the observations of Braun & Birch (2008) only span this set of modes and, therefore, we only estimate kernels for this subset of modes. Clearly, for the stress-free boundary condition, the absorption coefficient due to the excitation of kink waves is larger than that due to the sausage waves. However, the maximal-flux boundary condition shows the reverse.

The absorption coefficients measured by Braun & Birch (2008) were obtained by averaging the holographic observations in azimuth around the observational pupil. Hence, their measurements are only sensitive to the  $m = 0$  waves. In order to compare our theoretical results with their observations, we should therefore only consider the excitation of the sausage mode. Figure 7 compares their observations with our  $m = 0$  absorption coefficient  $\alpha_{\parallel,n}$ , which results solely from the excitation of sausage waves. The solid curves are our theoretical findings and the symbols correspond to the measurements of Braun & Birch (2008). The results for the stress-free and maximal-flux boundary conditions bracket the observations. It is quite likely

that the physical processes that occur near the surface of *real* solar plages are somewhere between the scenarios represented by these two extreme boundary conditions. Hence, despite the lack of exact agreement between the theory and the observations, it is reasonable to infer from Figure 7 that the excitation of tube waves is a significant mechanism for the absorption of  $p$ -mode energy by magnetic regions such as plage.

## 7. DISCUSSION

We have theoretically calculated the absorption coefficient of  $p$  modes for a simulated plage by the application of a weak scattering assumption. The plage is composed of an ensemble of magnetic fibrils, each treated as a vertical, axisymmetric, thin flux tube. Each of the tubes is pummeled by incident  $p$  modes within the solar convection zone, thereby exciting sausage and kink waves along the length of the flux tube. These tube waves propagate up and down the tubes carrying energy out of the acoustic cavity, thus damping the  $p$  modes.

Our computations indicate that this absorption mechanism can easily generate absorption coefficients in excess of 10%. When compared to observations of the absorption coefficient within plage obtained with ridge-filtered holography (Braun & Birch 2008), we find that the level of agreement between the observations and theory varies depending on the photospheric boundary condition that we adopt within the thin flux tubes (see Figure 7). A stress-free photospheric boundary produces

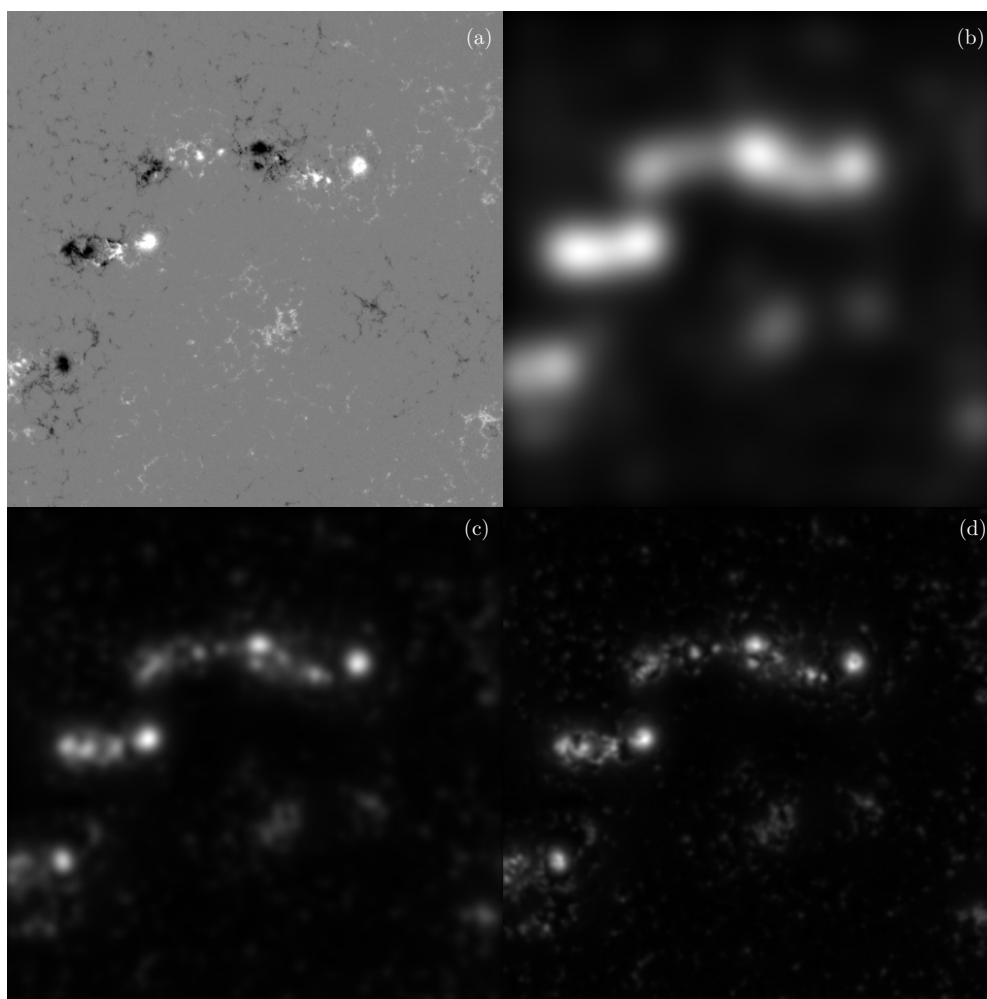


**Figure 4.** Images of the (a) magnetogram for a  $60^\circ \times 60^\circ$  area of the Sun taken 2002 April 1 with the MDI instrument. The remaining panels are convolutions of the modulus of the magnetogram with three different estimated kernels for waves on the  $p_4$  ridge with frequencies of (b) 2 mHz, (c) 3.5 mHz, and (d) 5 mHz.

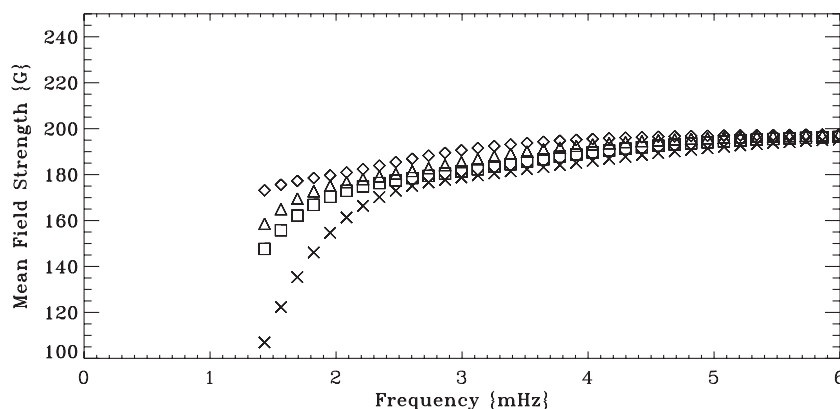


**Figure 5.** Field strength smoothed with the kernel and then averaged over all pixels within plage. The four different symbols correspond to kernels for waves of different mode orders: diamonds ( $p_1$ ), triangles ( $p_2$ ), squares ( $p_3$ ), and crosses ( $p_4$ ). For most frequencies the mean field strength falls just below 200 G; however, for sufficiently low frequency the kernels acquire sufficient spatial extent that quiet Sun begins to fill the kernel domain and reduce the mean field strength significantly.

insufficient absorption, whereas a maximal-flux boundary produces an excess. For frequencies greater than 4 mHz, the observations show a rapid decline in the absorption coefficient with almost zero absorption above 5 mHz. The theoretical curves begin to saturate as well (above 5 mHz for the stress-free boundary and above 3 mHz for the maximal-flux boundary); but lack the same sharp fall-off as shown by observations. These two boundary conditions bracket the range of possible reflectivities and the

reality is likely to lie in between. The saturation is not observed in the absorption coefficient for a single tube (Figures 1–3). Therefore, for both of these boundary conditions, the saturation at high frequency is a result of the decrease in the number of tubes that fall within the averaging kernel. This occurs naturally, since the horizontal wavelength of the  $p$  mode decreases with frequency and the resulting kernel shrinks in horizontal extent with increasing frequency.

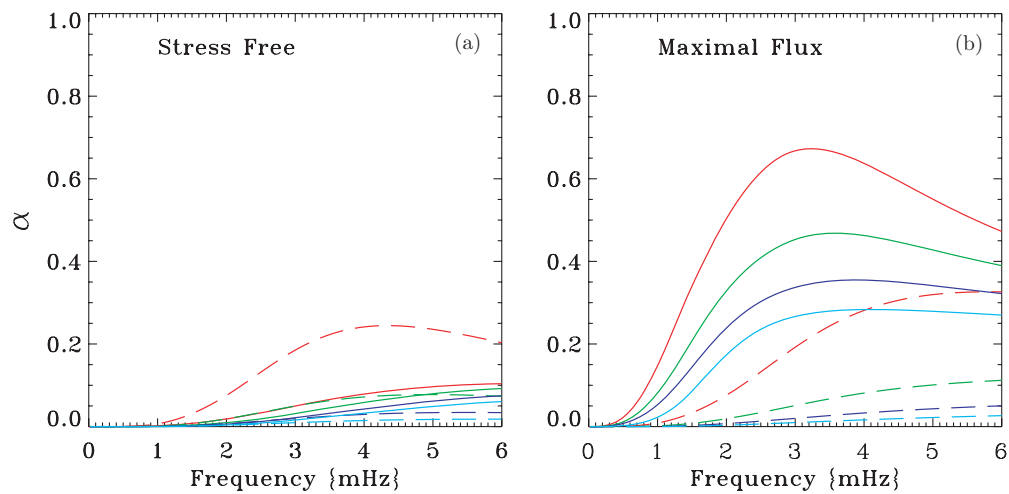


**Figure 6.** The absorption coefficient for  $m = 0$  (solid curves) and the sum of  $m = -1$  and  $m = 1$  (dashed curves) for the simulated plage. The plage is composed of thin flux tubes with  $\beta = 1$ . The four colors correspond to different mode orders: red ( $p_1$ ), green ( $p_2$ ), blue ( $p_3$ ) and aqua ( $p_4$ ). (A color version of this figure is available in the online journal.)

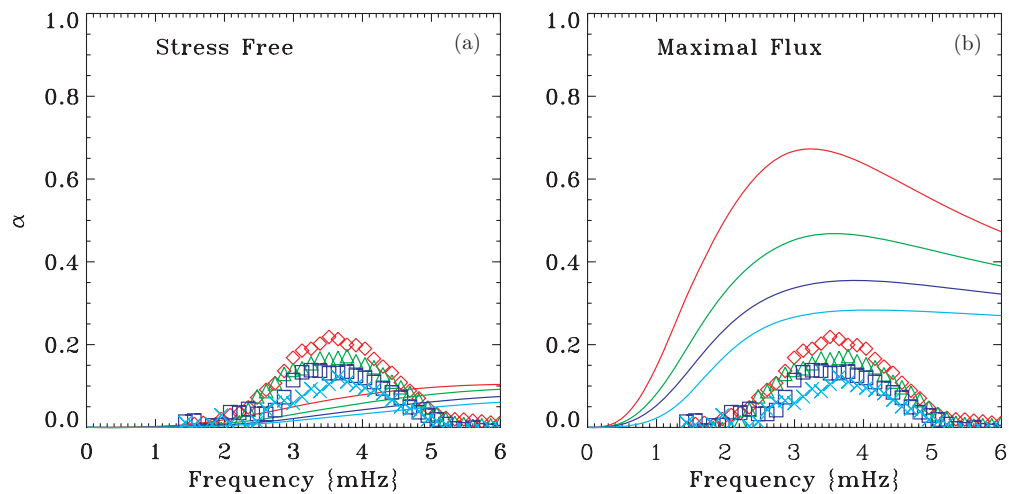


**Figure 7.** Absorption coefficient for  $m = 0$  for simulated plage (solid curves) is compared with observations (symbols). The plage is composed of thin flux tubes with  $\beta = 1$ . The four colors correspond to different mode orders: red ( $p_1$ ), green ( $p_2$ ), blue ( $p_3$ ), and aqua ( $p_4$ ). The symbols are observational results obtained using ridge-filtered holography (Braun & Birch 2008) for the same four mode orders. (A color version of this figure is available in the online journal.)

### 7.1. Systematic Errors in the Observations

When comparing the theoretical estimates and the observational results for the absorption coefficient in plage, one must keep in mind the systematic errors in the observations. In particular, the measured absorption coefficient samples not only absorption, but potentially emission as well. The differences between the frequency dependence of the absorption coefficients measured with Fourier–Hankel decomposition (e.g., Braun 1995) and ridge-filtered holography have been attributed to the different ways in which the two techniques sample the halo of emission that surrounds active regions (Lindsey & Braun 1999). The high-frequency portion of the spectrum is singularly susceptible to contamination, since the halo power peaks at 6 mHz. Furthermore, absorption can be effectively masked in observation if the lifetime of waves is sufficiently short that the waves do not travel completely across the observational domain before being absorbed, damped or scattered. For these reasons, Braun & Birch (2008) doubt that the fall-off that occurs in their observation beyond 4 mHz is real.

### 7.2. Weaknesses of the Calculation

There are also several issues that might cause problems for the theoretically derived absorption coefficients. The primary is a poor approximation for the observational kernel. Our choice of a Gaussian form for this calculation is physically reasonable and probably reproduces the core of the kernel well; however, it is less likely to match in the wings. The effect of a poor choice for a kernel is a poor assessment of the total number of tubes that should be included in the calculation for the absorption coefficient. If our approximation for the kernel has wider wings than the real kernel, our calculation will overestimate the number of tubes by integrating magnetic flux over a broader area than the observations, resulting in an overly large theoretical absorption coefficient. This problem can be exacerbated by the presence of nearby umbrae which increase the flux dramatically if oversampled. We would also like to note that without accurate calculations of the observational kernel it is difficult to assess the exact magnitude and the frequency dependence of the observed absorption in the *plage* since umbral contamination from nearby

sunspots could well lie within the kernel averaging function. We also ignored the treatment of energy carried downward by the acoustic jacket modes in our theoretically derived absorption coefficients. This requires further investigation.

A final weakness in our calculation is the weak scattering approximation where we assume that the flux tubes are non-interacting and that multiple scattering is unimportant. Since the absorption coefficient for our simulated plage can reach values as large as 70% (see Figure 7(b)), this assumption is clearly suspect. A proper treatment would require a full multiple-scattering calculation. Such calculations are notoriously difficult, and the results strongly depend on the mean separation of scatters. We will delay such a calculation for a later paper.

### 7.3. Destructive Interference Nulls

For tubes with low plasma  $\beta$  and with a reflecting photospheric boundary (i.e., stress free), nulls in the absorption coefficient appear in the range of observed helioseismic frequencies. These nulls arise because at certain frequencies total destructive interference occurs between the waves that are generated by the  $p$ -mode driving and propagate downward and those waves that propagate upward and are then reflected downward by the photospheric boundary condition. Since, no energy escapes the cavity, the absorption coefficient vanishes at these special frequencies. Such absorptive nulls occur for tubes with all values of  $\beta$ ; however, for larger values, the nulls occur at extremely high frequency and outside the helioseismic frequency range. Even if the photosphere truly acted as a completely reflecting surface, these nulls are unlikely to result in a strong observational signature within a plage. Unlike our simulated plage, real plage lacks a uniformity of tube sizes and strengths. Therefore, the absorptive nulls for different tubes will occur at different frequencies and the collective behavior of the tubes will be an average response where the nulls have been filled in.

### 7.4. Resonant Absorption

The mechanism of acoustic energy absorption that we have examined here is similar in some ways to resonant absorption. Since the tubes in our model are stratified and reside in a stratified atmosphere, it is impossible for a true resonance to occur where the wavelength along the tube interface is the same for both the incident acoustic wave and the internal magnetosonic wave. However, the interaction integrals,  $\mathcal{I}_{\parallel}(\omega)$  and  $\mathcal{I}_{\perp}(\omega)$ , can be maximized by matching the tube wave solution with the incident  $p$ -mode eigenfunction as closely as possible. The largest values of course occur when the nonmagnetic and magnetic wave forms have similar (if not identical) vertical wavelengths.

### 7.5. Conclusions

We have demonstrated that  $p$ -mode buffeting of thin flux tubes can generate a significant flux of longitudinal (sausage) or transverse (kink) waves. The energy carried by these tube waves, and thereby removed from the incident  $p$  mode, can result in large absorption coefficients. Our estimates for a plage region can reach well over 50% for some boundary conditions and low mode orders. Unlike absorption models for sunspots using mode conversion, significant absorption is achieved without the existence of substantial horizontal magnetic field. We find that our theoretical estimates are qualitatively similar to the observations at low frequency where the observations are trustworthy. Both the theoretical and observational absorption coefficients increase rapidly with frequency reaching a maximum or saturation value near 4 mHz. Above 4 mHz, the observations and theory behave quite differently. The observations show a rapid fall-off of the absorption coefficient with frequency, whereas our calculations reveal only a gentle decline. We suspect that the discrepancy lies in the observations which underestimate the absorption, because of the existence of high-frequency halos and finite lifetime effects.

We thank G. Vasil for helpful discussions on issues dealing with multiple scattering. R.J. acknowledges funding from Engineering and Physical Sciences Research Council, grant EP/C548795/1. B.W.H. acknowledges support from NASA through grants NNG05GM83G, NNX08AJ08G and NNX08AQ28G. We also thank the anonymous referee for useful comments.

### REFERENCES

- Abramowitz, M., & Stegun, I. A. 1964, *Handbook of Mathematical Functions* (New York: Dover)
- Bogdan, T. J., & Cally, P. S. 1995, *ApJ*, **453**, 919
- Bogdan, T. J., Hindman, B. W., Cally, P. S., & Charbonneau, P. 1996, *ApJ*, **465**, 406 (BHCC)
- Braun, D. C. 1995, *ApJ*, **451**, 859
- Braun, D. C., & Birch, A. C. 2008, *Sol. Phys.*, **251**, 267
- Braun, D. C., Duvall, T. L., Jr., & LaBonte, B. J. 1987, *ApJ*, **319**, L27
- Braun, D. C., Duvall, T. L., Jr., & LaBonte, B. J. 1988, *ApJ*, **335**, 1015
- Cally, P. S. 2000, *Sol. Phys.*, **192**, 395
- Cally, P. S., & Bogdan, T. J. 1993, *ApJ*, **402**, 732
- Crouch, A. D., & Cally, P. S. 2003, *Sol. Phys.*, **214**, 2011
- D'Silva, S. 1994, *ApJ*, **435**, 881
- Fan, Y., Braun, D. C., & Chou, D.-Y. 1995, *ApJ*, **451**, 877
- Hanasoge, S. M., Birch, A. C., Bogdan, T. J., & Gizon, L. 2008, *ApJ*, **680**, 774
- Hindman, B. W., & Jain, R. 2008, *ApJ*, **677**, 769 (Paper I)
- Hollweg, J. V. 1988, *ApJ*, **335**, 1005
- Keppens, R., Bogdan, T. J., & Goossens, M. 1994, *ApJ*, **436**, 372
- Lindsey, C., & Braun, D. C. 1999, *ApJ*, **510**, 494
- Lou, Y.-Q. 1990, *ApJ*, **350**, 452
- Maltby, P., Avrett, E. H., Carlsson, M., Kjeldseth-Moe, O., Kurucz, R. L., & Loeser, R. 1986, *ApJ*, **306**, 284
- Rosenthal, C. S. 1992, *Sol. Phys.*, **139**, 25